LAWRENCE
LIVERMORE
NATIONAL
LABORATORY

UCRL-JRNL-220790

Solid Deuterium-Tritium Surface Roughness In A Beryllium Inertial Confinement Fusion Shell

B. J. Kozioziemski, J. D. Sater, J. D. Moody, D. S. Montgomery, C. Gautier

April 21, 2006

Journal of Applied Physics

Solid deuterium-tritium surface roughness in a beryllium inertial confinement fusion shell

B. J. Kozioziemski, J. D. Sater, and J. D. Moody

Lawrence Livermore National Laboratory, Livermore CA 94551

D. S. Montgomery and C. Gautier

Physics Division, Los Alamos National Laboratory, Los Alamos, NM 87545

(Dated: March 24, 2006)

Abstract

Solid deuterium-tritium (D-T) fuel layers for inertial confinement fusion experiments were formed inside of a 2 mm diameter beryllium shell and were characterized using phase-contrast enhanced x-ray imaging. The solid D-T surface roughness is found to be 0.4 μm for modes 7-128 at 1.5 K below the melting temperature. The layer roughness is found to increase with decreasing temperature, in agreement with previous visible light characterization studies. However, phase-contrast enhanced x-ray imaging provides a more robust surface roughness measurement than visible light methods. The new x-ray imaging results demonstrate clearly that the surface roughness decreases with time for solid D-T layers held at 1.5 K below the melting temperature.

PACS numbers:

INTRODUCTION

Inertial confinement fusion experiments, such as those at the University of Rochester Omega Laboratory for Laser Energetics (LLE) and planned for the Lawrence Livermore National Laboratory National Ignition Facility (NIF) compress fuel layers to the high density and pressures required for fusion to occur. A mixture of deuterium and tritium (D-T) is used as the fuel because of its high fusion cross section. An ablator surrounds the fuel, which serves the dual role of containing the cryogenic solid D-T fuel and to push the fuel layer during compression. One ignition target design for the NIF has an ablator which is a 2 mm diameter, 150 μm wall beryllium shell doped with approximately 1% copper.[1, 2] Successful ignition experiments require both the ablator and fuel layers to be smooth and uniformly thick spherical shells.[2]

Copped-doped beryllium Be(Cu) shells are produced by sputter deposition on a spherical mandrel and subsequently mechanically polished.[3] D-T solidifies at 19.7 K with a vapor pressure of 140 torr, thus effectively eliminating the option of mechanical machining or polishing. Instead, a process termed beta-layering is used to achieve less than 1 μm root-mean-square (RMS) roughness specification. This process was first demonstrated using toroidal geometries[4–6] and subsequently shown to produce smooth solid D-T layers in optically transparent plastic spherical shells appropriate for NIF.[7, 8] Additional layering studies of the solid hydrogen isotopes use enhanced layering methods, such as infrared heating, to produce smooth surfaces.[9–11]. Experiments have shown that the layer roughness increases as the solid temperature is reduced from the melting temperature to the design temperature of 1.5 K below the melting temperature.[10]

Beryllium shells are preferred over the plastic shells for NIF ignition experiments because their higher density results in lower Rayleigh-Taylor hydrodynamic instability growth. However, characterization of solid D-T layers inside the optically opaque beryllium shell has proven difficult.[12–14] It was recently suggested[15] and demonstrated[16, 17] that solid D-T could be characterized using phase-contrast enhanced x-ray imaging. However, those early experiments could not resolve the fine scale roughness necessary to meet NIF characterization requirements. This paper describes new experiments with improved x-ray imaging resolution that convincingly demonstrate that D-T layers in beryllium shells meet the NIF surface roughness specification. The roughness of several solid D-T layers was measured as the temperature was reduced from near the melting temperature to several kelvin lower. We find that the roughness increases as the solid temperature is reduced at rates of 2 mK/min and faster. We find that the cooling-induced roughness

decreases (anneals) when held at a constant temperature, although the roughness does not return to the pre-cooled value.

EXPERIMENTAL METHOD

Phase-contrast x-ray imaging

The x-ray opacity of Be(Cu) is 10 000 times larger than solid D-T for x-ray energies sufficient to penetrate the Be(Cu) shell. However, the real part of the solid D-T refractive index is within a factor of 10 of the Be(Cu) value. This suggests that phase-sensitive imaging methods[18–20], can be used for characterization of the solid D-T inside of the Be(Cu) shell.[15] The simplest such method is the free-space propagation technique, which has been discussed extensively in the literature.[21–29] Briefly, a plane-wave or spherical-wave with high spatial coherence is incident on the object under study. Features in the object that correspond to sharp changes in the wave phase refract and diffract the x-rays. The detector must be located far enough from the object that the small angular deflection of the x-rays translates to image contrast. The free-space propagation method has been shown by calculation and experiment to render the solid D-T surface visible.[15, 17] The first experimental images lacked the resolution and signal-to-noise ratio required to perform accurate surface roughness analysis. The imaging system has since been improved by making changes in both the x-ray source and detector.

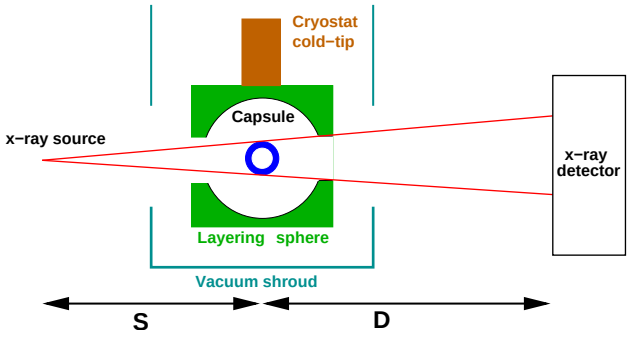

FIG. 1: Experimental geometry. An x-ray source is located a distance S from a beryllium shell suspended in a spherical cavity. The cavity is machined in an aluminum cube and attached to the cold-tip of a liquid-helium flow cryostat. An x-ray detector is located a distance D from the shell.

A direct-detection x-ray microscope, using an X-ray CCD camera to detect the x-ray photons, was used to collect the images in this paper. A schematic of the imaging geometry is shown

in Fig. 1. The direct-detection system uses a Cu-anode Thermo-Kevex PSX5-927 micro-focus source. It has been designed to provide a minimum x-ray spot size of 4-5 μm when operated at 45 kV accelerating potential between 2 and 4 Watts. This small spot size provides the high spatial coherence required for phase-contrast imaging. Furthermore, the Cu spectrum is ideally suited for characterization of the solid D-T layer inside of the Be(Cu) shell because the Cu K-α emission line is just below the Cu absorption edge.

A Princeton Instruments X-ray CCD camera is used to acquire the direct-detection images. The CCD chip is 1024x1024 pixels, with a pixel pitch of 25 μm. The dark current is minimized by cooling the CCD to -30° C. The full-well capacity is approximately 400 000 electrons per pixel. This corresponds to approximately 180 detected 8 keV x-ray photons per pixel at saturation. Averaging multiple frames improves the photon signal-to-noise ratio. The source-to-object distance and object-detector distances for the direct-detection case are 73 mm and 685 mm. This geometry provides the 10x geometric magnification required to fill the full field of view of the CCD.

Accurate characterization of the solid D-T roughness requires a sufficient signal-to-noise ratio (SNR), as will be discussed. With the direct-detection method, the SNR is improved by acquiring multiple image frames. Liquid helium flowing though the cryostat causes up to 5 μm of movement of the shell on a time scale of 60 seconds. The 6 second exposure time used in the direct-detection was short compared to the cryostat movement. Successive frames are aligned before adding to minimize the motional blurring.

The sputtered beryllium shell used in these experiments was one of the first produced. Since the process was not yet optimized at the time of production, surface and bulk defects are present in the shell. These defects imprint in the x-ray images and in some cases obscure the D-T solid–vapor interface. The analysis is improved by subtracting an image of the empty beryllium shell. This removes the beryllium shell defects from the image of the shell with a D-T layer, making the D-T surface easier to locate.

Solid D-T layer formation

The Be shell is suspended inside of a spherical cavity machined out of an aluminum cube. This is attached to the cold-tip of an ARS LT3-B liquid helium cooled flow cryostat. At the operating temperature, the shell is conductively cooled by 1 torr of ^{4}He gas in the cavity. The temperature of the aluminum cube is monitored using two calibrated germanium resistance thermometers.

Temperature is controlled at the cold tip by a Neocera LTC21 temperature controller. A diode thermometer is the input source and a 35 W heater is the control element. Temperature control was within $\pm$ 5 mK of the set-point at the cold tip on a time scale of 10 seconds. The thermal mass of the aluminum cube damped its temperature oscillations to less than $\pm$ 2 mK.

Liquid D-T is condensed into the shell through a fill tube. The fill tube is approximately 50 μm OD, 20 μm ID where it enters the 70 μm OD mechanically drilled hole through the Be. The fill-tube is attached to the Be shell with Tra-Con TRA-BOND 2115 epoxy. A small leak near the fill tube, possibly due to a crack formed during the drilling, necessitated a rather large epoxy joint to seal the shell. The D-T source is a palladium bed, which acts as a constant pressure source.[30] The D-T is slowly admitted into the shell until the desired amount is obtained. Then the cryostat is quickly cooled to freeze solid D-T in the segment of the line that passes through the cryostat cold-tip, effectively trapping a fixed amount of D-T in the shell.

There is no thermometer on the Be shell. Rather, the temperature is monitored on the aluminum cube. The shell temperature is higher than the surrounding layering cavity because of the D-T self heating. For the temperature range, and hence ^{4}He pressure, under study, the temperature difference between the shell and the aluminum cube is treated as constant. The temperature of the shell is calibrated relative to the aluminum cube by noting when the D-T is almost completely melted. The temperature on the layering sphere is noted, and all measurements are reported relative to this last melting temperature, T_m. Typically, there is a 240 mK temperature difference between the shell and the layering sphere, which is consistent with the published value of ^{4}He thermal conductivity.

It has been found that smooth layers are formed by slowly cooling through the melt.[8, 10] A similar procedure was followed for these experiments. Starting with the temperature well below T_m, where the D-T is completely solid, the shell temperature is slowly raised until the solid has completely melted. The shell is then cooled at a rate of either 1 mK/60 s or 1 mK/120 s to 0.4 K below T_m. Complete solidification of the D-T is observed to occur at approximately 0.1 K below T_m. Once the solid temperature reaches 0.4 K below T_m, the cooling rate is increased to a range of 2 mK/min - 8 mK/min. For those cases where the temperature ramp rate required multiple days of observation, the temperature ramp was slowed significantly over night.

CHARACTERIZATION OF SOLID D-T ROUGHNESS

Figure 2 shows a 2D image of a solid D-T layer inside the Be shell taken with the direct-detection imaging system. The outer Be radius, R_{Be}, the interface between the solid D-T and the Be, R_I, and the D-T solid–vapor interface, R_{DT} are indicated by the arrows in the image. Each interface is located by a sharp intensity variation due to the phase-contrast enhancement. Figure 3 shows an intensity lineout across the D-T solid–vapor interface. The images are analyzed for the D-T surface roughness by determining the radial position of the interface as a function of angular position θ. Roughness is quantified by calculating the root-mean-square (RMS) deviation and the Fourier transform power spectrum of $R_{DT}(\theta)$.

Two different methods for determining $R_{DT}(\theta)$ give the same results for the D-T surface quality. The first uses a non-linear least-squares fit to a functional form approximating the edge shape, as shown in Fig. 3. The second determines the radial position that gives the maximum correlation with a reference shape. Both provide similar levels of accuracy in determining the $R_{DT}(\theta)$. The correlation method is more robust for the cases where the images had significant noise, or in which the surface roughness decreased the edge contrast. Details for the two methods are described below.

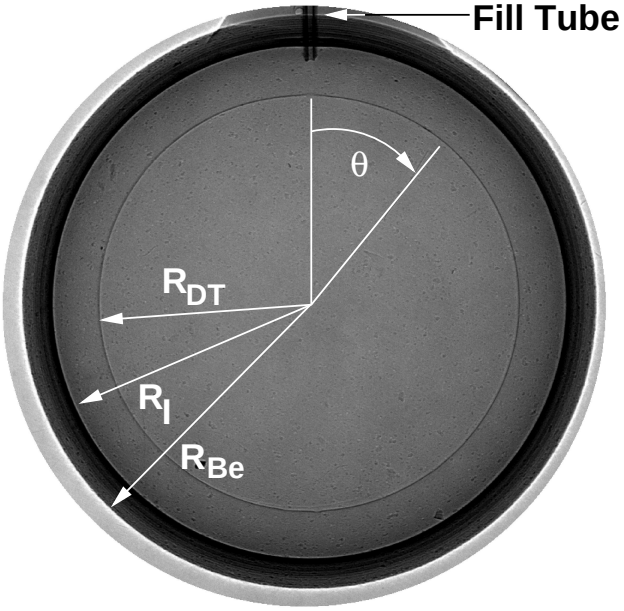

FIG. 2: Solid D-T layer inside of the copper-doped beryllium shell. The shell is at 18.2K.

Functional fit

The edge detection can be performed using a non-linear least-squares fit to the radial intensity profile at each θ position. The intensity profile is very similar to a Gaussian derivative, except that the peak and valley do not have identical amplitudes. A slightly modified function,

$$f(r) = a_1 \exp(-(a_6 r - a_2)^2/a_3)(r - a_2) + a_4 + a_5 r, \quad (1)$$

where a_i are the fitting coefficients and r is the radial position, approximates the intensity profile near the solid D-T surface. When a_6 is unity, $f(r)$ reduces to the Gaussian derivative. A value of a_6 less than unity forces the peak amplitude to be less than the valley while a_6 greater than unity makes the peak amplitude greater than the valley. Typical values of a_6 for the data in this paper are 0.95 to 0.98. The fitting parameters a_4 and a_5 allow fitting with the increasing absorption of the beryllium shell as the radius increases. a_1, a_2, and a_3 adjust the overall amplitude, center, and width of the intensity feature, respectively. Panel (a) of Fig. 3 shows a typical experimental intensity profile near the solid D-T interface as a function of radial position and the corresponding fit using Eq. 1. The fit using $f(r)$ matches the shape of the intensity profile.

$\mathrm{R_{DT}}(\theta)$ is taken to be the value of a_2 for quantification of the roughness. a_2 does not exactly correspond to the absolute position of the solid–vapor interface, but does follow the relative variations of the interface position as a function of θ. Simulated images show that the D-T solid–vapor interface is located closer to the valley rather than the mid-point between the peak and valley.

Correlation method

The second method for determining the surface roughness follows the relative surface position by determining the maximum correlation. First, a radial intensity profile containing the D-T solid–vapor interface is selected from the data set to serve as the template. Then the correlation of the template with the intensity profile at a particular θ is calculated according to

$$C_j(\theta) = \sum_{i=1}^{n} T_i I_{i+j}(\theta), \quad (2)$$

where T_i is the template intensity at pixel i and $I_{i+j}(\theta)$ is the intensity for the θ slice. The maximum value of $C_j(\theta)$ calculated for a range of integer shifts j corresponds to the shift j required

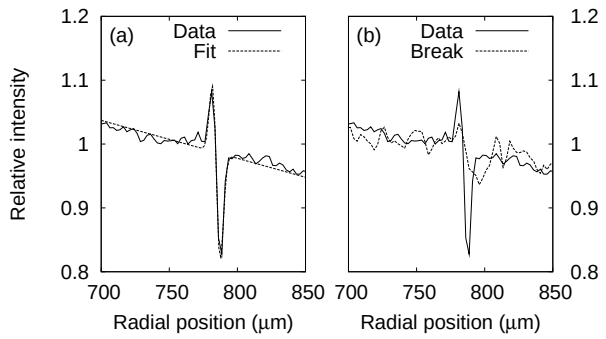

FIG. 3: Normalized intensity profile across the solid–vapor D-T boundary as a function of radial position. The left panel (a) shows a typical experimental data profile across a smooth D-T solid–vapor interface and the best fit to the experimental intensity using Eq. 1. The dashed line in the right panel (b) shows the intensity variation near a large surface perturbation. The roughness decreases the contrast at the interface considerably compared to a relatively smooth surface.

to make the sampled data match the template. Sub-pixel correlation is obtained by interpolating T and I using a spline fit. The correlation is calculated this way for each θ. As with the functional fitting method, the result is the relative shift of the D-T solid–vapor interface as a function of θ, from which the RMS roughness and power spectrum can be calculated.

The functional fitting and correlation method were compared for a number of experimental and simulated data sets. The methods produce equivalent results when the solid–vapor interface is marked by a high SNR ratio intensity transition. With a low SNR image, the functional fitting fails to converge in some cases. The correlation method will always find a maximum over the specified search range. However, that maximum may be in error, due to the noise. Therefore, it is important to determine the SNR ratio necessary for accurate surface roughness characterization.

Required signal-to-noise ratio

The measured D-T layer roughness is the sum of two components. The first is the power representative of the actual D-T surface roughness. The second part is the mode power due to noise and systematic imperfections in the measurement system. Systematic imperfections include distortions in the optics, camera tilt, and variations in the pixel spacing. Only the instrument noise will be considered here. The result of instrument noise is that it limits the edge detection accuracy and hence creates a noise floor in the measured power spectrum. The noise floor is a

constant power level independent of mode number and is the power spectrum that is obtained from a perfectly smooth D-T layer in the absence of systematic detector imperfections. Understanding the noise floor is important since it sets an absolute lower limit to the mode power that can be detected.

A numerical model to simulate the effect of noise on locating the D-T solid–vapor interface in the x-ray phase-contrast images was developed. Noise consistent with a real CCD was superimposed on a simulated image consistent with the experimental D-T interface. The detector is modeled as a 1024 x1024 array with each element capable of representing integer values between 0 and 2^N -1. N is the number of bits available in the detector, where N = 16 is used in the following discussion. Two sources of noise are included in the model. The first is shot noise due to the x-ray photons that strike the detector. A Poisson distribution is used to model the shot noise. The second noise source is the CCD readout noise, which is modeled as a Gaussian distribution. A realistic detector has a typical standard deviation of σ_e = 12 electrons at each pixel per image read. Shot noise dominates this experiment because each x-ray photon generates many electrons. Dark current noise is not included in this model because the dark current produced by this cooled CCD is several orders of magnitude below the other sources of noise.

The solid–vapor interface intensity signal is modeled as a Gaussian derivative, as expressed in Eq. 1. The signal amplitude is defined as the peak-to-valley amplitude of the Gaussian derivative. For this model, a_1 sets the peak-to-valley amplitude, a_4 is the average number of detected photons, a_5 is set to zero, and a_6 is set to unity. The value for the peak-to-valley width, determined by a_3, is set to a width of 2 pixels to match the experimental measurement, where each pixel is 2.3 μm square. Then the total number of counts in a pixel at position r is given by the sum of the signal and the noise terms. The noise level can be adjusted to simulate averaging multiple images. Figure 4 shows a simulated radial intensity profile for two different SNR levels. The left panel corresponds to a single direct-detection acquisition, and the right panel corresponds to averaging 20 acquisitions.

Multiple-frame images were analysed by averaging a number of single-frame images and computing the power spectrum of the simulate constant radius solid–vapor D-T interface. Figure 5 shows the noise floor obtained for the specified number of frame averages. Also shown is the maximum allowable mode power at mode 128 in the NIF D-T surface roughness specification. Comparison of the simulation results with the NIF specification indicates that a minimum of five frame averages are required to verify that the D-T surface meets the specification. The power

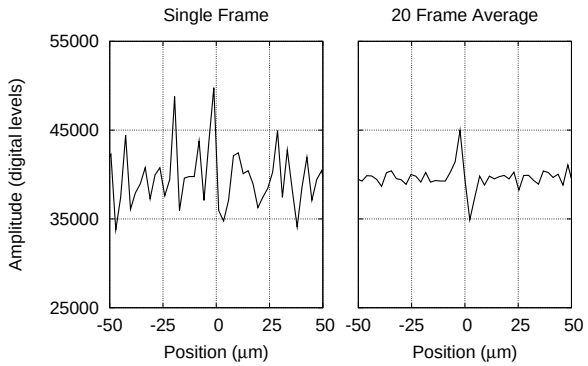

FIG. 4: Radial intensity profile in a simulated phase-contrast enhanced x-ray image of the D-T solid–vapor interface. The left panel shows a single frame, while the right is a 20 frame average.

spectra reported in this article were obtained from images consisting of 20 frames to set the noise floor about a factor of 10 lower than the required minimum.

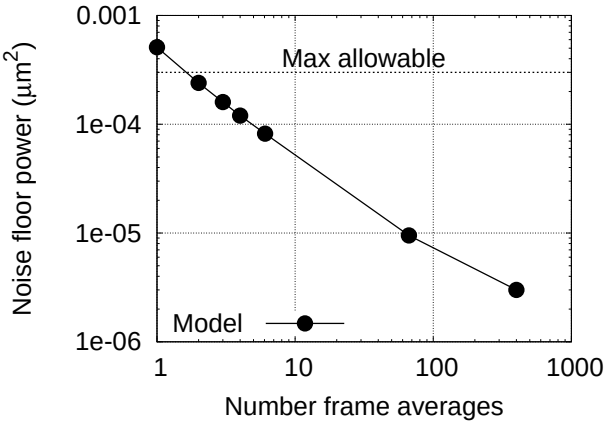

FIG. 5: Decrease in power spectrum noise fbor with increasing image averages. The model includes realistic noise comparable to the experimental data. The maximum allowable noise fbor for successful characterization of NIF fuel layers requires a minimum of 5 frame averages. Using 20 frames reduces the noise further.

D-T LAYER ROUGHNESS

Previous experiments have shown that the solid D-T roughness depends on the cooling rate, the solid temperature, and the time since freezing. We explored each of these for the solid D-T layer in the beryllium shell. Layers were formed by slowly cooling through the melting temperature.

Then the layers were cooled to ΔT = 1.5 K using different rates for each layer. The roughness and power spectra were computed for each of the layers at several temperatures while cooling.

This particular beryllium shell has a large epoxy joint securing the fill-tube to the shell. The epoxy causes a localized temperature perturbation, and hence solid D-T thickness variation. This thickness perturbation increases the roughness power in the first few modes of the Fourier analysis over what is expected for an isothermal shell surface. Therefore, the first few modes in the power spectrum are not representative of the intrinsic D-T layer roughness. A previous study with the same shell and a smaller epoxy joint had less power in the low modes.[17] The slope of the roughness power spectrum changes between modes 5 and 7 in the current data and indicates roughness dominated by the epoxy joint transitioning to the inherent surface roughness. Therefore, only modes greater than 7 will be included in the RMS sum and analysis.

Layer roughness vs temperature

Figure 6 shows the RMS roughness in modes 7-128 for four D-T layers. The data points in Fig. 6 labeled X-ray #1-3 are for D-T layers formed in the beryllium shell and characterized with x-ray imaging. The Vis. #1 data is from a D-T layer inside a plastic shell characterized using visible light from a previous experiment. The visible light and x-ray characterizations produce similar roughness over the small temperature range where the two can be compared. X-ray results will be discussed first and compared to the visible light method later.

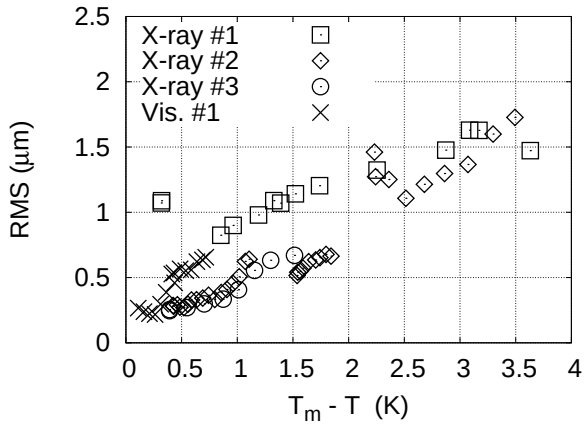

FIG. 6: Measured RMS roughness in modes 7 through 128 for one several D-T layers. Three of the data runs used a 186 μm thick D-T layer in the Be shell, characterized with the x-ray imaging. The Vis. #1 data set was for a 100 μm thick D-T layer in a plastic shell, imaged with visible light.

Each data set has a similar increase in roughness for ΔT greater than 0.5 K. Differences between the layers are due to the initial layer formation and temperature histories. In particular, there is a decrease in the RMS between 0.3 K and 0.8 K for X-ray #1 that is not present in the other layers. This is because a flat spot formed during its initial freeze. The flat spot size decreased, due to beta-layering, during the slow cooling of the layer at a rate of 0.62 mK/min to ΔT = 0.8 K. At this point, the cooling rate was increased to 3.7 mK/min. The subsequent increase in roughness is distributed over the entire layer and is not localized to the one flat spot.

The X-ray #2 layer, open diamonds, was cooled from the melting temperature to ΔT = 0.4 K at 0.46 mK/min. Then the cooling rate was increased to 1.86 mK/min from ΔT = 0.4 K to 1.1 K. There was a consistent increase in roughness over this range. When the layer reached ΔT = 1.1 K, the cooling rate was decreased to 0.43 mK/min until the layer reached ΔT = 1.5 K. During this much slower portion of the temperature ramp, the layer roughness decreased slightly. The cooling rate was increased to 2 mK/min between 1.5 K and 1.8 K, and resulted in a slight increase in roughness over this temperature range. Between 1.8 K and 2.2 K, the cooling rate was slowed to 0.31 mK/min. Even with the very slow cooling rate, the layer roughens considerably while cooling to ΔT = 2.2 K.

The X-ray #3 layer, open circles, was formed by cooling at 0.46 K/min from the melting temperature to ΔT = 0.4 K. At that point, the cooling rate was increased to 7.45 mK/min until ΔT reached 1.5 K. This layer RMS increase is very similar to the X-ray #2 layer with the 1.86 mK/min cooling rate.

Finally, the Vis. #1 layer was cooled much more slowly, at a rate of 0.25 mK/min, from the melt to ΔT = 1.5 K. Data is only shown for this layer down to ΔT = 0.72 K because it becomes too rough to reliably characterize using visible light.

The D-T surface power spectrum for modes 7 - 128 required for NIF ignition is shown in figure 7 along with the measured spectra for D-T layers at ΔT = 0.39 K and ΔT = 1.52 K. At ΔT = 0.39 K, the power spectrum is well below that at ΔT = 1.52K. The power spectrum for the layer at ΔT = 1.52 K, on average, meets the NIF ignition specification. Furthermore, the power spectrum for the layer at ΔT = 0.39 K demonstrates that the x-ray imaging method is capable of characterizing the layers with sufficient accuracy for NIF ignition experiments.

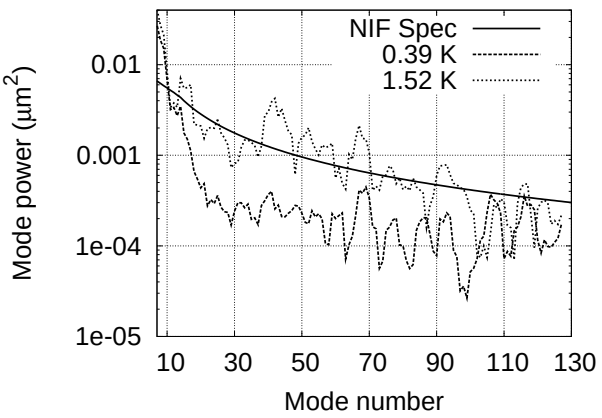

FIG. 7: Required NIF ignition power spectrum for a D-T layer 1.5 K below the melting temperature (solid line) and the measured power spectra for one particular layer at two different temperatures. The layer roughness increases as ΔT increases, but still follows the NIF specification at ΔT = 1.52 K. The measured power spectra data was smoothed using a boxcar average four modes wide to make the trends readily apparent.

Layer roughness versus cooling rate

It is advantageous to produce D-T layers at ΔT = 1.5 K as quickly as possible for ICF ignition experiments. However, previous experiments have shown that D-T layers grown by slow–cooling are smoother. Therefore, it is necessary to determine the optimum cooling rate that produces ignition quality layers in the shortest time.

Several different cooling rates were studied at different points in the layering process. The layers are initially formed by cooling from the liquid at rates of 0.46 mK/min to 0.6 mK/min. This is often the most critical part of the layer formation process, when the cooling rate needs to be the slowest. The cooling rate was increased substantially for $\Delta T > 0.4$ K, when the layer is sufficiently below the melting temperature. Figure 6 shows two layers, X-ray #2 and X-ray #3, which were formed with the same cooling rate of 0.46 mK/min and had similar initial roughness. At ΔT = 0.4 K, the rates were increased to 1.86 mK/min and 7.45 mK/min, respectively. Both show similar roughness increase to ΔT = 1.1 K, the point where the cooling rate of X-ray #2 was reduced significantly.

Figure 6 also showed one layer, X-ray #2, where the temperature ramp was slowed to 0.43 mK/min between 1.1 and 1.5 K. The roughness decreases slightly over this range. Therefore, it

appears that cooling at a rate approximately 0.43 mK/min is slow enough that the beta-layering process can heal the surface roughness generated while cooling. Similarly, from the X-ray #2 data, it appears that this is true only to about ΔT = 1.8 K, since the roughness increased considerably while cooled at 0.31 mK/min from 1.8 to 2.2 K.

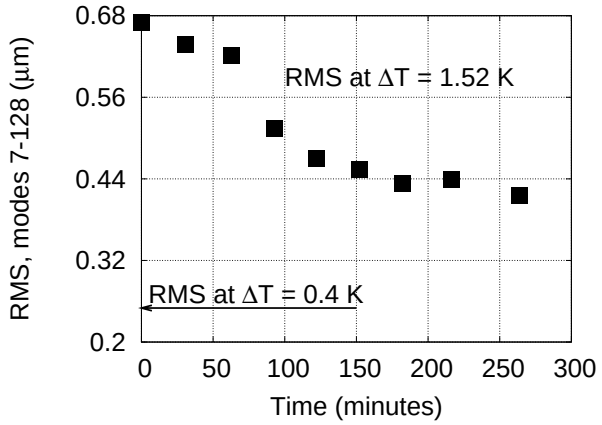

FIG. 8: The RMS for modes 7-128 for a layer that was cooled to ΔT = 1.52 K below the freezing temperature, then held at that temperature. The RMS decreases with time, but does not reach the initial ΔT = 0.4 K roughness minimum of 0.25 μm.

Figure 8 shows the RMS in modes 7-128 from X-ray #3 taken as the layer was held at ΔT = 1.52 K. The RMS decreases from the maximum value of 0.67 μm to 0.41 μm over 260 minutes, with most of the change occurring within the first 100 minutes. The roughness does not return to the minimum layer RMS value of 0.25 μm at ΔT = 0.4 K, but does decrease by 40% from the maximum of 0.68 μm obtained just after reaching ΔT = 1.52 K. Power in all of the modes decreased and no mode or mode ranges were favored in the smoothing. Much of the roughness appears in the form of cracks at the surface. The cracks are visible throughout the layer image as the layer reaches ΔT = 1.52 K, but quickly become small enough to no longer be visible in the image.

Cracks

There are positions in the image where features form that appear to be cracks. Figure 9 shows an example of the unwrapped surface for layer X-ray #3 at three temperatures. For the surfaces, the contrast at the D-T interface drops considerably near “cracks”, with visible gaps in the edge

in some cases. These cracks are possibly due to the thermal contraction of the solid. Cracks were observed to form as the layer was cooled at a rate of 7.45 mK/min from 0.5 to 1.5 K below the melting temperature. As pointed out earlier, the cracks healed when the layer was held at ΔT = 1.52 K. The cracks were very prominent for $\Delta T > 2$ K and did not heal over time. This results suggest that the beta-layer process is able to heal cracks to ΔT = 1.52 K, but not past ΔT = 2 K.

The cracks in the D-T layer makes the analysis of the layer roughness difficult because the sharp phase change at the crack can strongly deflect the incident x-rays. Figure 9 shows an example of a D-T layer at three different temperatures. The images have been unwrapped to present the D-T surface as a straight line. At ΔT = 0.96 K, panel (a), the D-T surface is continuous and can be followed along the entire length. As the temperature is lowered to ΔT = 1.52 K, panel (b), the surface remains continuous, but the contrast is reduced at one point. The dashed line in the right panel (b) of Fig. 3 shows the line profile across one such feature. While the edge can be located in the radial profile, the uncertainty in the position is larger than for the data at a smooth surface. Finally, at ΔT = 3.96 K, multiple breaks and bifurcations are present at the D-T surface. The surface roughness is large enough that features outside of the center-plane contribute to, or degrade, the image contrast. Simply following the intensity transition is not sufficient to accurately characterize the layer roughness. The edge detection becomes unreliable at these points, and may interpolate over the broken region, leading to what appears to be a smoother surface in the analysis. Thus, the measured RMS possibly under-represents the real surface roughness for these surfaces. A more advanced analysis method would include both the position and contrast variations in the calculation of the roughness. However, the signal-to-noise at present is too low to reliably employ the contrast variations. Furthermore, if the layer RMS roughness in modes 7-128 is greater than 1.5μm, the layer would be unacceptable for NIF ignition experiments.

DISCUSSION

Comparison to visible light methods

Previous experiments have studied D-T layer formation in optically transparent plastic shells. Characterization in these studies was performed using the visible light shadowgraphy method.[31, 32] However, because the visible light is strongly refracted at defects on the D-T layer, the shadowgraphy method cannot accurately track the D-T layer roughness when cracks are present in the

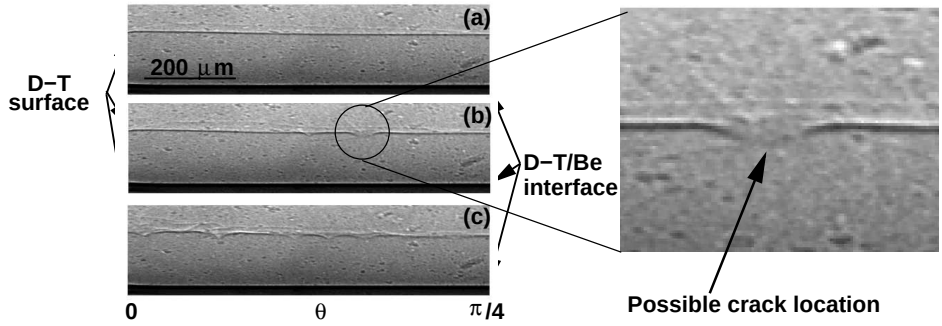

FIG. 9: Three unwrapped image segments of a solid D-T layer in the Be shell as the layer is cooled. They are at temperatures (a) 0.96 K, (b) 1.52 K, and (c) 3.96 K below the triple point temperature. Breaks in the edge are apparent as the layer is cooled. The right image show a magnified view near a possible crack at the solid–vapor interface.

layer. Figure 6 shows one such shadowgraph analysis. The layer roughness can only be reliably tracked to ΔT = 0.7 K, or about 0.7 μm RMS for modes 7-128. At this point, breaks in the edge appeared. No breaks appear in the x-ray image edge until the roughness approaches 1-1.5 μm, and layers have been taken to ΔT = 2.0 K.

The roughness for both the shadowgraph and x-ray images are comparable where they overlap in temperature. Also, the temperature at which the shadowgraph becomes unreliable is close to the temperature in the X-ray #2 and X-ray #3 layers where the slope of the RMS vs temperature begins to increase. This observation, combined with previous modeling results[17] provides confidence that the x-ray imaging accurately characterizes rough surfaces.

CONCLUSIONS

Several D-T layers were formed inside of a beryllium shell and characterized using x-ray phase-contrast enhanced imaging. The direct-detection imaging using a micro-focus Cu anode x-ray source greatly improved upon earlier results using a scintillator for the imaging.[17] These recent images demonstrate that the surface roughness of the D-T layer can be accurately characterized using the x-ray phase-contrast enhanced imaging.

These results show that the best D-T layer grown in this beryllium shell at ΔT = 1.5 K would meet the roughness specification for NIF ignition experiments. The RMS roughness for modes 7-128 at ΔT = 1.5 K is 0.41 μm, which meets the NIF surface roughness specification. Each of

the layers formed in this shell became rougher as it was cooled to ΔT = 1.5 K below the melting temperature. Cooling at a rate of 7.45 mK/min, followed by keeping the temperature constant at ΔT = 1.5 K, produced a layer with nearly the same roughness as one that was cooled at a significantly slower rate. Cooling at rates of 0.43 mK/min or slower between ΔT = 1.1 K and ΔT = 1.5 K is slow enough that roughness induced by the cooling is less than the smoothing by beta-layering.

This work was performed under the auspices of the U.S. Department of Energy by the University of California, Lawrence Livermore National Laboratory under contract No. W-7405-Eng-48 and by the Los Alamos National Laboratory under contract No. W-7405-Eng-36.

[1] D. C. Wilson, P. A. Bradley, N. M. Hoffman, F. J. Swenson, D. P. Smitherman, R. E. Chrien, R. W. Margevicius, D. J. Thoma, L. R. Foreman, J. K. Hoffer, et al., Physics of Plasmas **5**, 1953 (1998).

[2] S. W. Haan, T. Dittrich, G. Strobel, S. Hatchett, D. Hinkel, M. Marinak, D. Munro, O. Jones, S. Pollaine, and L. Suter, Fusion Technology **41**, 164 (2002).

[3] R. McEachern, C. Alford, R. Cook, D. Makowiecki, and R. Wallace, Fusion Technology **31**, 435 (1997).

[4] J. K. Hoffer and L. R. Foreman, Phys. Rev. Lett. **60**, 1310 (1988).

[5] J. K. Hoffer and L. R. Foreman, J. Vac. Sci. Technol. A **7**, 1161 (1989).

[6] J. K. Hoffer, L. R. Foreman, J. J. Sanchez, E. R. Mapoles, and J. D. Sheliak, Fusion Tech. **30**, 529 (1996).

[7] A. J. Martin, R. J. Simms, and R. B. Jacobs, J. Vac. Sci. Technol. A **6**, 1885 (1988).

[8] J. Sater, B. Kozioziemski, G. W. Collins, E. R. Mapoles, J. Pipes, J. Burmann, and T. P. Bernat, Fusion Tech. **35**, 229 (1998).

[9] D. N. Bittner, G. W. Collins, E. Monsler, and S. Letts, Fusion Technology **35**, 244 (1999).

[10] D. N. Bittner, G. W. Collins, and J. D. Sater, Fusion Science and Technology **44**, 749 (2003).

[11] C. Stoeckl, C. Chiritescu, J. A. Delettrez, R. Epstein, V. Y. Glubov, D. R. Harding, R. L. Keck, S. J. Loucks, L. D. Lund, R. L. McCrory, et al., Physics of Plasmas **9**, 2195 (2002).

[12] T. J. Asaki, Fusion Technology **35**, 126 (1999).

[13] T. J. Asaki, J. K. Hoffer, and J. D. Sheliak, Fusion Technology **33**, 171 (1998).

[14] T. Hale, T. Asaki, K. Telschow, and J. Hoffer, in *SPIE-Int. Soc. Opt. Eng. Proceedings of Spie - the*

International Society for Optical Engineering, edited by R. H. Bossi and D. M. Pepper (SPIE, San Antonio, TX, USA, 1998), vol. 3399, pp. 97–108.

[15] D. S. Montgomery, A. Nobile, and P. J. Walsh, Review of Scientific Instruments **75**, 3986 (2004).

[16] B. J. Kozioziemski, J. A. Koch, A. Barty, H. E. Martz, Jr., W.-K. Lee, and K. Fezzaa, Journal of Applied Physics **97**, 063103 (2005).

[17] B. J. Kozioziemski, J. D. Sater, J. D. Moody, J. J. Sanchez, R. A. London, A. Barty, H. E. Martz, and D. S. Montgomery, Journal of Applied Physics **98**, 103105 (2005).

[18] V. A. Bushuev, E. A. Beliaevskaya, and V. N. Ingal, Il Nuovo Cimento D. **19**, 513 (1997).

[19] P. Cloetens, R. Barrett, J. Baruchel, J.-P. Guigay, and M. Schlenker, J. Phys. D **29**, 133 (1996).

[20] R. Fitzgerald, Physics Today **53**, 23 (2000).

[21] S. W. Wilkins, T. E. Gureyev, D. Gao, A. Pogany, and A. W. Stevenson, Nature **384**, 335 (1996).

[22] A. Snigirev, I. Snigireva, V. Kohn, S. Kuznetsov, and I. Schelokov, Rev. Sci. Inst. **66**, 5486 (1995).

[23] B. E. Allman, P. J. McMahon, J. B. Tiller, K. A. Nugent, D. Paganin, A. Barty, I. McNulty, S. P. Frigo, Y. Wang, and C. C. Retsch, J. Opt. Soc. Am. A **17**, 1732 (2000).

[24] K. A. Nugent, T. E. Gureyev, D. F. Cookson, D. Paganin, and Z. Barnea, Phys. Rev. Lett. **77**, 2961 (1996).

[25] A. Pogany, D. Gao, and S. W. Wilkins, Review of Scientific Instruments **68**, 2774 (1997).

[26] T. E. Gureyev, C. Raven, A. Snigirev, I. Snigireva, and S. W. Wilkins, J. Phys. D. **32**, 563 (1999).

[27] T. E. Gureyev and S. W. Wilkins, J. Opt. Soc. Am. A **15**, 579 (1998).

[28] S. C. Mayo, T. J. Davis, T. E. Gureyev, P. R. Miller, D. Paganin, A. Pogany, A. W. Stevenson, and S. W. Wilkins, Optics Express **11**, 2289 (2003).

[29] D. Paganin and K. A. Nugent, Phys. Rev. Lett. **80**, 2586 (1998).

[30] E. R. Mapoles, J. Sater, J. Pipes, and E. Monsler, Phys. Rev. E **55**, 3473 (1997).

[31] J. A. Koch, T. P. Bernat, G. W. Collins, B. A. Hammel, B. J. Kozioziemski, A. J. MacKinnon, J. D. Sater, D. N. Bittner, and Y. Lee, Fusion Technology **38**, 123 (2000).

[32] J. A. Koch, T. P. Bernat, G. W. Collins, B. A. Hammel, J. D. Sater, and D. N. Bittner, Fusion Science and Technology **43**, 55 (2003).